





Transverse cardiac slicing and optical imaging for analysis of transmural gradients in membrane potential and Ca²⁺ transients in murine heart

Q. Wen¹, K. Gandhi², Rebecca A. Capel³, G. Hao⁴, C. O'Shea⁵, G. Neagu³, S. Pearcey³, D. Pavlovic⁵ , Derek A. Terrar³, J. Wu¹, G. Faggian² , Patrizia Camelliti⁶  and M. Lei^{3,4} 

¹Institution of Cardiology, Union Hospital, Tongji Medical College, Huazhong University of Science and Technology, Wuhan, China

²Medical School, University of Verona, Verona, Italy

³Department of Pharmacology, University of Oxford, Oxford, UK

⁴Key Laboratory of Medical Electrophysiology of Ministry of Education, Collaborative Innovation Center for Prevention and Treatment of Cardiovascular Disease/Institute of Cardiovascular Research, Southwest Medical University, Luzhou, 6400, China

⁵Institute of Cardiovascular Sciences, University of Birmingham, Birmingham, UK

⁶School of Biosciences and Medicine, University of Surrey, Guildford, UK

Edited by: Don Bers & Jamie Vandenberg

Key points

- A robust cardiac slicing approach was developed for optical mapping of transmural gradients in transmembrane potential (V_m) and intracellular Ca²⁺ transient (CaT) of murine heart.
- Significant transmural gradients in V_m and CaT were observed in the left ventricle.
- Frequency-dependent action potentials and CaT alternans were observed in all ventricular regions with rapid pacing, with significantly greater incidence in the endocardium than epicardium.
- The observations demonstrate the feasibility of our new approach to cardiac slicing for systematic analysis of intrinsic transmural and regional gradients in V_m and CaT.

Abstract Transmural and regional gradients in membrane potential and Ca²⁺ transient in the murine heart are largely unexplored. Here, we developed and validated a robust approach which combines transverse ultra-thin cardiac slices and high resolution optical mapping to enable systematic analysis of transmural and regional gradients in transmembrane potential (V_m) and intracellular Ca²⁺ transient (CaT) across the entire murine ventricles. The voltage dye RH237 or Ca²⁺ dye Rhod-2 AM were loaded through the coronary circulation using a Langendorff perfusion system. Short-axis slices (300 μ m thick) were prepared from the entire ventricles (from the apex to the base) by using a high-precision vibratome. Action potentials (APs) and CaTs

Q. Wen graduated from Tongji medical school Huazhong University of Science and Technology as a Medical Doctor in May 2015. Since graduating, he has worked at the Cardiology Department of Union Hospital, specialising in diagnosis and treatment of hypertension, CAD and heart failure. He studies the association of SNPs of IL33/ST2 signal pathway and CAD, hypertension and diabetes in the Chinese population. He translated for the 8th Central Congress Cardiology. His hobbies are reading, body building and playing basketball. **Kushal Gandhi** earned his PhD through a collaboration between the University of Verona, Italy and the University of Oxford, UK. He is now working as a postdoctoral researcher at Texas Tech University Health Sciences Center at the Permian Basin, Odessa, TX, USA. His work now focuses on the endocannabinoid system (ECS), which is dysregulated by irregular diet during pregnancy and affects future generations. ECS is vital for appetite and pain regulation, neurological development and other physiological processes in humans.



Q. Wen and K. Gandhi are joint first authors. J. Wu, G. Faggian, P. Camelliti and M. Lei are joint senior authors.

were recorded with optical mapping during steady-state baseline and rapid pacing. Significant transmural gradients in V_m and CaT were observed in the left ventricle, with longer AP duration (APD₅₀ and APD₇₅) and CaT duration (CaTD₅₀ and CaTD₇₅) in the endocardium compared with that in the epicardium. No significant regional gradients were observed along the apico-basal axis of the left ventricle. Interventricular gradients were detected with significantly shorter APD₅₀, APD₇₅ and CaTD₅₀ in the right ventricle compared with left ventricle and ventricular septum. During rapid pacing, AP and CaT alternans were observed in most ventricular regions, with significantly greater incidence in the endocardium in comparison with epicardium. In conclusion, these observations demonstrate the feasibility of our new approach to cardiac slicing for systematic analysis of intrinsic transmural and regional gradients in V_m and CaT in murine ventricular tissue.

(Received 11 April 2018; accepted after revision 12 June 2018; first published online 21 June 2018)

Corresponding author M. Lei: Department of Pharmacology, University of Oxford, Mansfield Road, OX1 3QT. Email: ming.lei@pharm.ox.ac.uk

Introduction

Because of its feasibility for genetic modification, the mouse has been the most popular animal species for modelling human disease conditions and for mechanistic research, as well as therapeutic exploration, despite distinct differences in its cardiac electrophysiological properties compared to the human heart, including marked differences in heart size, heart rates and action potential waveforms. The mouse is also the second mammalian species, after humans (Lander *et al.* 2001), in which a substantial amount of genomic information has been analysed (Waterston *et al.* 2002). Within the cardiovascular research community, the mouse has been widely used for exploring molecular, cellular and systemic mechanisms underlying inherited and acquired ventricular arrhythmic diseases (Nerbonne, 2014). As transgenic technology has advanced, mutagenesis has become much easier to carry out in mice and an increasing number of genetically modified mouse systems have been generated for the study of cardiac arrhythmias (Sabir *et al.* 2008). The models include ion channelopathies with minimal structural abnormalities, and those of structural heart disease (Choy *et al.* 2016). The former group includes catecholaminergic polymorphic ventricular tachycardia (CPVT) (Wehrens *et al.* 2003), the long (Wu *et al.* 2012) and short QT syndromes (LQTS and SQTs), and Brugada syndrome (BrS) (Papadatos *et al.* 2002; Choy *et al.* 2016). The latter group includes several types of cardiomyopathies, such as arrhythmogenic right ventricular dysplasia (ARVD) (Asano *et al.* 2004), dilated cardiomyopathy (DCM) and hypertrophic cardiomyopathy (HCM) (Choy *et al.* 2016).

Surprisingly, despite the popularity of mouse models in heart research, little is known about murine heart transmural and regional electrophysiological heterogeneities such as action potential and Ca²⁺ transient characteristics. These are vitally important for phenotypic and mechanistic research

into cardiac disease conditions, in particular cardiac arrhythmias. In this species, the transmural and regional electrophysiological heterogeneities have been largely unexplored.

Thin tissue slices, a well-established experimental preparation for electrophysiological studies of the brain, have recently emerged as a promising model for cardiac electrophysiology investigations. Thin slices, prepared from the ventricle of a number of different species (Halbach *et al.* 2006; Bussek *et al.* 2009; Camelliti *et al.* 2011; Wang *et al.* 2014), have been shown to retain structural and functional properties of the native myocardium, including tissue architecture, cell type ratio, cell distribution, cell–cell electrical and mechanical coupling, and extracellular matrix (Bussek *et al.* 2009; Camelliti *et al.* 2011). Importantly, cardiac slices exhibit similar electrophysiological characteristics to the intact heart and respond to the application of pharmacological compounds similarly to the whole heart (Camelliti *et al.* 2011; Himmel *et al.* 2012), thus providing a promising experimental model for electrophysiology, Ca²⁺ handling, and drug action investigations.

Most previous electrophysiology studies on cardiac slices have employed low spatial resolution recording methods, including patch clamp (Burnashev *et al.* 1990), sharp electrodes (Halbach *et al.* 2006; Bussek *et al.* 2009; Himmel *et al.* 2012) and low-density multi-electrode arrays (Bussek *et al.* 2009; Camelliti *et al.* 2011). Higher spatial resolution methods, such as optical mapping, provide exciting opportunities to monitor dynamic cellular electrophysiological events as they occur in real time (Wang *et al.* 2015; Kang *et al.* 2016). Furthermore, prior studies have been limited to the analysis of sub-epicardial (Wang *et al.* 2015) or sub-endocardial tangentially cut slices (Kang *et al.* 2016), or a few transmurally cut slices (Bussek *et al.* 2009), an approach inadequate for accurate capture of regional and transmural cardiac electrophysiological properties. A method

for systematic analysis of regional and transmural electrophysiological heterogeneities across the whole ventricles in mouse is currently missing.

In order to address the issues described above, in the present study we developed a feasible transverse slicing method and combined it with a high-throughput optical imaging technique as a new approach for studying cellular electrophysiology of murine heart in intact sliced ventricular tissue. These transverse slices were cut at right angles to the long axis of the heart. Our approach enables, for the first time, the use of a series of slices prepared from ventricle to measure transmembrane potential (V_m) and intracellular Ca^{2+} transient (CaT) with high temporal and spatial resolution, allowing (i) comparison of successive slices which form a stack representing the original geometry of the heart; (ii) profiling of the transmural and regional gradients in V_m and CaT in the ventricle; (iii) characterisation of transmural and regional profiles of action potential and CaT alternans.

Methods

Ethical approval

All animal experiments were performed on adult mice (CD1, 12–20 weeks old) in accordance with the United Kingdom Animals (Scientific Procedures) Act 1986 and were approved by the University of Oxford Pharmacology ethical committee (approval ref. PPL: 30–3340) and the national guidelines under which the institution operates. All mice used in this study were maintained in a pathogen-free facility at the University of Oxford. Mice were given *ad libitum* access to food and water. The authors confirm that they have taken all steps to minimise the animals' pain and suffering. Our work complies with the journal policy and regulations (Grundy, 2015).

Heart isolation

Mice were killed by cervical dislocation in accordance with Schedule 1 killing method. Hearts were rapidly excised and Langendorff-perfused with oxygenated Krebs solution (containing in mM: NaCl 119, $NaHCO_3$ 25, sodium pyruvate 1.8, KH_2PO_4 1.2, KCl 4.7, $MgCl_2$ 1.0, $CaCl_2$ 1.8, and glucose 10; equilibrated with 95% O_2 /5% CO_2 , pH 7.4) at 37°C and at constant rate of 3.5–4 ml/min for 10 min. To prevent formation of blood clots in the coronary circulatory system, animals were treated with heparin (200 units) under non-recovery terminal general anaesthesia by injection of an overdose of 1.2% Avertin solution (0.5–0.8 ml i.p. (2,2,2-tribromoethanol, Sigma-Aldrich Poole, Dorset, UK) prior to killing and hearts were injected with streptokinase (400 units) via

the coronary system after organ excision according to approved procedure by the Home Office.

Dye loading

Fluorescent dyes were loaded via the coronary circulation during Langendorff perfusion, applied by injection into the aortic cannula. The voltage sensitive dye RH237 (Thermo Fisher Scientific, UK) was delivered as a 15 μ l bolus of 2 mM concentration, injected into the cannula in small volume steps over a period of 5 min. The Ca^{2+} dye Rhod-2 AM (Thermo Fisher Scientific, UK) was administered as a 50 μ l bolus (stock solution: 1 mg/ml in DMSO) over a 5 min period, and recirculated for 45 min in the presence of 0.5 mM probenecid. After dye loading, hearts were perfused with Krebs solution containing 10 μ M blebbistatin, a myosin II inhibitor used to stop contractions and avoid movement artefacts during optical mapping recordings.

Slice preparation

Table 1 summarises the slice preparation procedure. Hearts were removed from the Langendorff set-up and dissected in cold (4°C) oxygenated (99.5% O_2) Tyrode solution (in mM: NaCl 140; KCl 4.7; glucose 10; HEPES 10; $MgCl_2$ 1; $CaCl_2$ 1.8; pH 7.4) containing the excitation–contraction uncoupler 2,3-butanedione monoxime (BDM, 10 mM). Atria and valves were removed using a sharp scalpel blade, leaving the ventricles intact. Ventricles were glued base-down (histoacryl tissue adhesive; Braun, Melsungen, Germany) onto a pre-made 4% agar block, previously fixed onto the vibratome specimen holder (VF-300 vibrating microtome; Precisionary Instruments Inc., Greenville, USA). Ventricles were subsequently embedded in 4% low-melt agarose and cooled on ice at 4°C. The specimen holder with agarose-embedded ventricles was mounted onto the stage of the vibratome filled with cold (4°C) oxygenated (99.5% O_2) Tyrode solution containing BDM. Short-axis slices were cut at a thickness of 100 μ m, 300 μ m or 500 μ m, using a razor blade at a speed of 0.02 mm/s and vibration frequency of 82 Hz. After initial experiments aiming to determine the best slice thickness for dye loading, dye retention and optical mapping recordings, short-axis slices of 300 μ m thickness were prepared from the entire ventricles (from the apex to the base) for the study of regional and transmural V_m and Ca^{2+} properties. As summarised in Table 1, the total cold ischaemic time during slicing is between 1.5 and 4 min. Slices were then transferred to recovery solutions for recovery in a pre-incubation chamber filled with Krebs solution containing 10 μ M blebbistatin at room temperature for

Table 1. Summary of the slicing and imaging protocol

	Dye loading	Perfusion	Slicing	Recovery 1	Recovery 2	Recovery 3	Pre-imaging	Imaging
Temperature	37°C	37°C	4°C	4°C	RT	RT	37°C	37°C
Solution	Krebs	Krebs	Tyrode	Tyrode	Krebs	Krebs	Krebs	Krebs
BDM (10 mM)	No	No	Yes	Yes	No	No	No	No
Blebbistatin (10 μ M)	No	Yes	No	No	Yes	Yes	Yes	Yes
Ca ²⁺	1.8 mM	1.8 mM	1.8 mM	1.8 mM	1.8 mM	1.8 mM	1.8mM	1.8mM
O ₂	95%	95%	100%	100%	95%	95%	95%	95%
CO ₂	5%	5%	0%	0%	5%	5%	5%	5%
Duration	5–7 min	20 min	1.5–4 min	10 min	10 min	5 min	3 min	<1 min

RT, room temperature; Krebs, Krebs-Henseleit solution; Tyrode, Tyrode solution.

30 min before electrophysiological investigations. To prevent tissue from curling, slices were collected on Sylgard blocks and held in position using a nylon mesh in the pre-incubation chamber.

Optical mapping

Slices were electrophysiologically assessed with the optical mapping method, using a custom-designed optical mapping system equipped with an EMCCD camera (Evolve 128 Photometrics, Tucson, AZ, USA). Figure 1F shows a schematic diagram of the mapping set-up. Slices were kept in Krebs solution containing 10 μ M blebbistatin at 37°C during imaging. Four 530 nm LEDs were used for excitation of the Ca²⁺-sensitive dye Rhod-2. CaT fluorescence was collected at 585 \pm 40 nm. For V_m signals, four 530 nm LEDs were used for excitation of RH237, and emission was collected using a 662 nm long pass filter. V_m and CaT measurements were taken at maximal resolution (128 \times 128 pixels; pixel area 47 \times 47 μ m) at

a rate of 1000 frames/s. Slices were electrically stimulated with bipolar pulses of 2 ms duration, at voltages 1.5 times above threshold (5–10 V) and initial frequency of 2 Hz. For AP and CaT alternans investigations, slices were stimulated at frequencies of 2, 4, 8 and 16 Hz.

Data analysis

AP duration (APD) and CaT duration (CaTD) were analysed using OPTIQ (program developed by Dr Burton, University of Glasgow). AP and CaT signals were filtered using a Gaussian spatial filter (radius 2 pixels) before relevant parameters were extracted. APD was measured as the time from the upstroke to 50% and 75% repolarisation (APD50 and APD75). Similarly, the CaTD was measured as the time from the upstroke to 50% and 75% recovery (CaTD50 and CaTD75). AP and CaT alternans are defined as the electrical or calcium transient discordant in duration or in amplitude. These phenomena depend on the underlying instability mechanisms (V_m -driven or CaT-driven)

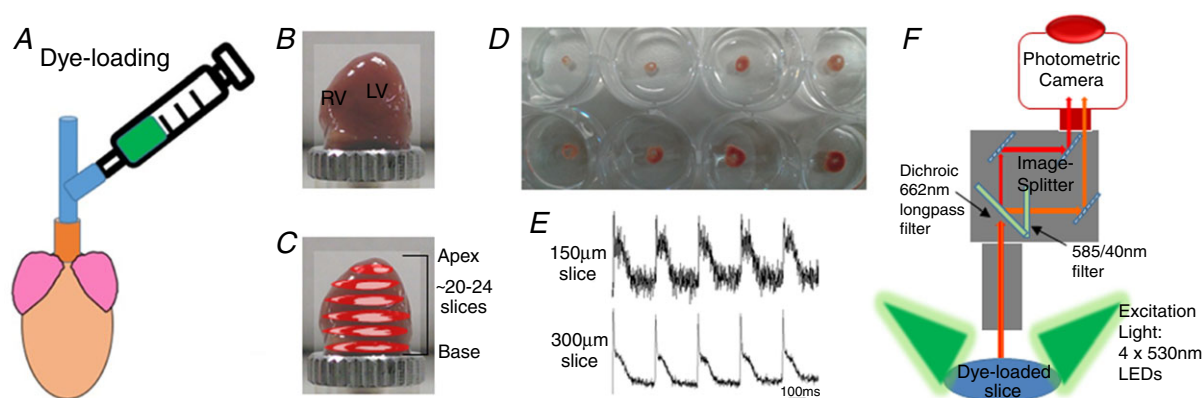


Figure 1. Optimisation of murine cardiac slice methodology

A, voltage (RH237) or calcium (Rhod-2 AM) dyes were loaded via coronary circulation using the Langendorff perfusion system. B, ventricles were embedded in 4% low-melt agarose and mounted onto the vibratome specimen holder. C, up to 24 transverse slices were cut from the apex to the base in ice-cold BDM Tyrode solution. D, slices were recovered at room temperature in Krebs solution containing 10 μ M blebbistatin for 30 min, before optical mapping studies. E, V_m signals in slices cut at 150 μ m and 300 μ m thickness. F, optical mapping setup with four 530 nm excitation LEDs and a 128 \times 128 EMCCD camera.

and the coupling between AP and CaT alternans cycling.

For assessment of conduction velocity (CV), the multi-vector polynomial method (Bayly *et al.* 1998) was used within bespoke analysis software, Electro-Map (O'Shea *et al.* 2017). Following Gaussian filtering (3×3 pixel area, $\sigma = 1.5$), activation maps, generated from measuring the time of the depolarisation midpoint, were spatially segmented into regions of 5×5 pixels. A polynomial surface was then fitted to local activation times to describe propagation in the area, and local CV quantified as the gradient vector of the polynomial surface. Mean CV was then calculated from the local CVs across the tissue slice.

Statistical analysis

Transmural and regional APD/CaTD distributions were analysed using a Student's paired *t* test or one-way ANOVA with *post hoc* Tukey's test and repeated measures correlation among tissue regions. Regional frequency-dependent AP/CaT alternans and arrhythmia heterogeneity were analysed using a chi-squared test. A value of $P < 0.05$ was considered statistically significant. Values are expressed as means \pm SEM.

Results

Optimisation of murine transverse ventricular slices for V_m and CaT measurements

Adult murine ventricular slices have been previously developed for electrophysiology applications (Halbach *et al.* 2006), but optimisation of the slice preparation to enable systematic analysis of V_m and CaT across the whole murine ventricles has yet to be achieved. Figure 1 illustrates the methodology implemented in this study. Critical steps included determination of an efficient dye loading method, a slice thickness able to maintain intact tissue morphology and generate optimal voltage and calcium signals, and a recovery period necessary to reach stable signals after slice preparation. As shown in Fig. 1, to achieve optimal dye loading, the voltage dye RH237 or Ca^{2+} dye Rhod-2 AM were loaded through the coronary circulation using the Langendorff perfusion system. Prevention of blood clot formation was essential for optimal dye loading and was achieved by initial injection of heparin (200 units) before killing, and subsequent injection of streptokinase (400 units) directly into the coronary system after heart excision. Ventricles were embedded in low-melting temperature agarose to provide structural support to the tissue during sectioning. Slices were cut at right angles to the long axis of the heart from the

apex to the base, and thicknesses from $100 \mu\text{m}$ to $500 \mu\text{m}$ were tested, with $300 \mu\text{m}$ found to be the best thickness to achieve optimal recordings for both V_m and CaT. Slices less than $300 \mu\text{m}$ thick showed markedly lower V_m and CaT signals (Fig. 1E), while slices thicker than $300 \mu\text{m}$ suffered from poor oxygenation. After preparation, slices were pre-incubated at room temperature in Krebs solution containing $10 \mu\text{M}$ blebbistatin for an optimal recovery time of 30 min, prior to electrophysiological assessment using a custom-designed optical mapping system (Fig. 1F). Figure 2 shows viable slices obtained with the optimised protocol, summarised in Table 1, and representative V_m and CaT signals from different regions, illustrating the robustness of this preparation for murine research. We monitored the 'rundown' of the V_m and CaT signals for up to 4 h, the average signal 'rundown' is less than 25%. Our experiments usually finished within 3 h.

Transmural and regional characteristics of V_m

After successful optimisation of the methodology, we tested the feasibility of combining murine slices with high resolution optical mapping for systematic transmural and regional profiling of V_m and CaT across the murine ventricles. Transverse slices ($300 \mu\text{m}$ thick) were prepared from the entire ventricles (from apex to base; Fig. 2A), and AP duration (APD) and CaT duration (CaTD) were mapped with high spatial and temporal resolution. Examples are shown in Fig. 2B corresponding to slice 10 shown in Fig. 2A.

Figure 3 summarises the distribution of APD at 50% repolarisation (APD50) and 75% repolarisation (APD75) across the entire murine ventricles at 2 Hz pacing frequency. Figure 3A and B show typical APD75 colour-coded maps and action potentials from a series of transverse ventricular slices, suggesting the presence of APD heterogeneities in the mouse ventricles. An important advantage of the cardiac slice model is the ability to study any region of the mouse ventricle and thus simultaneously investigate transmural, apico-basal (apex–base), and interventricular APD gradients. As shown in Fig. 3C, there are significant transmural gradients in APD50 and APD75 in the left ventricle at 2 Hz pacing frequency (Fig. 3Ca and c), with the shortest APDs occurring in the epicardium and the longest APDs occurring in the endocardium (APD50: Epi 50 ± 7 ms, Endo 58 ± 8 ms, $P < 0.01$; APD75: Epi 71 ± 8 ms, Endo 83 ± 8 ms, $P = 0.0001$, paired *t* test; $n = 5$ hearts). Differences between longest and shortest APD (transmural APD dispersion) in LV free wall were 8 ± 1 ms at APD50 and 11 ± 1 ms at APD75. Importantly transmural heterogeneities were not restricted to a particular region of the left ventricle, but were present along the entire left ventricle free wall from the apex to the base (Fig. 3Ca

and *c*), with the highest transmural APD dispersion occurring in the apical region (apex transmural dispersion: 16 ± 1 ms at APD75; $P < 0.05$, one-way ANOVA comparing apex-centre-base transmural dispersion).

In addition to transmural APD distribution, cardiac slices allowed us to investigate APD gradients across the apico-basal axis of the left ventricle free wall. As shown in Fig. 3*Ca* and *c*, there is no significant apico-basal gradient in APD50 and APD75 in either epicardium or endocardium ($P > 0.05$, one-way ANOVA with *post hoc* Tukey's test; $n = 5$ hearts).

Finally, as each slice contains left ventricle free wall, right ventricle and septum, we were able to assess inter-ventricular APD gradients. As shown in Fig. 3*Cb* and *d*, there are significant interventricular differences in APD50 and APD75 at the base and centre, but not at the apex. APD was shorter in the right ventricle in comparison to the left ventricle and the septum, in the basal and centre regions ($P < 0.05$, one-way ANOVA with *post hoc* Tukey's test; $n = 5$ hearts), with interventricular APD75 dispersion of 23 ± 6 ms and 13 ± 3 ms, respectively.

Transmural and regional characteristics of CaT

Analysis of transmural and regional heterogeneity in calcium handling are summarised in Fig. 4. Figure 4*A* and *B* show representative maps of CaT duration (CaTD) at 75% recovery (CaTD75) from apical, centre and basal ventricular mouse slices during electrical pacing at 2 Hz frequency (Fig. 4*A*), and typical optical CaT recordings from corresponding regions (Fig. 4*B*). As shown in Fig. 4*C*, there are significant transmural gradients in CaTD at 50% recovery (CaTD50) in apical, centre and basal regions of the left ventricle free wall at 2 Hz pacing frequency (Fig. 4*Ca*), with significantly longer CaTD50 in the endocardium compared to the epicardium (apex: 13% longer, $P < 0.01$; centre: 8%, $P < 0.05$; base: 10%, $P < 0.01$; $n = 6-8$ hearts). A significant transmural gradient in CaTD75 (Fig. 4*Cc*) was also observed in the basal and centre regions of the left ventricle ($P < 0.05$, paired *t* test; $n = 5-7$ hearts), but not in the apical region.

We further assessed the distribution of CaTD along the apico-basal axis of the left ventricle free wall. As shown in Fig. 4*Ca* and *c*, no significant apico-basal gradient in

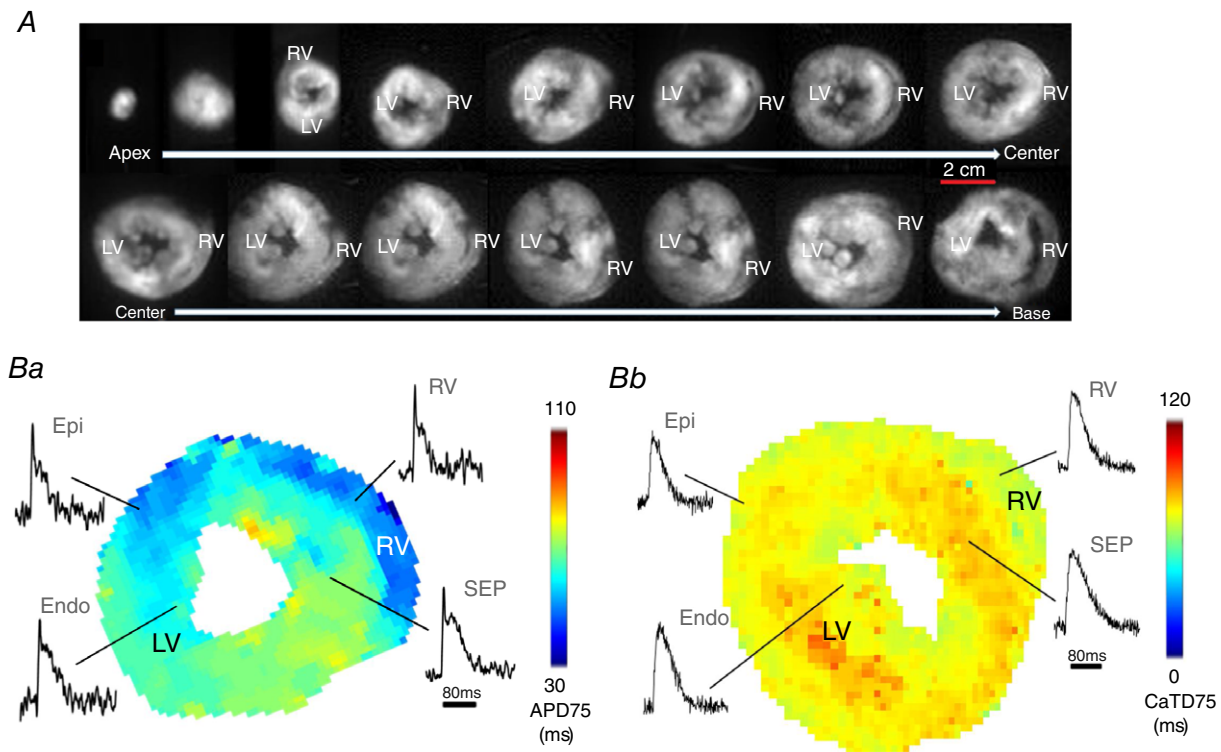


Figure 2. V_m and CaT measurements in murine ventricular slices

A, bright field images of transverse ventricular slices ($300 \mu\text{m}$ thick) prepared from both ventricles of a mouse heart (from the apex to the base). Scale bar: 2 cm. *B*, AP duration (APD; *Ba*) and CaT duration (CaTD; *Bb*) maps generated from a slice prepared from the central region of the ventricles, with raw AP and CaT signals acquired from the epicardium (Epi) and endocardium (Endo) of the left ventricle, the ventricular septum (SEP) and the right ventricle (RV). APD scale bar: 80 ms.

CaTD50 and CaTD75 was observed in the murine left ventricle ($P > 0.05$, one-way ANOVA; $n = 5-7$ hearts).

Finally, we compared CaTD measured in left ventricle free wall regions with CaTD recorded in right ventricle and ventricular septum regions for each tissue slice, to investigate interventricular CaTD gradients. As shown in Fig. 4Cb and d, there are significant regional differences in CaTD50 but not CaTD75 at the apex and base, with the shortest CaTD50 occurring in the right ventricle, and an interventricular CaTD50 dispersion of 4 ± 1 ms and 6 ± 1 ms at the apex and base, respectively ($n = 6-7$ hearts).

Transmural and regional heterogeneity of frequency-dependent AP and CaT alternans

Further experiments were carried out to assess the feasibility of using murine transverse ventricular slices and optical mapping to characterise transmural and regional

differences in frequency-dependent AP and CaT alternans and arrhythmias. Slices were paced at frequencies of 2, 4, 8 and 16 Hz, and AP and CaT were recorded at each frequency (Figs 5A and 7A). As shown in Figs 5 and 7, AP and CaT alternans and arrhythmic events often occurred at higher pacing frequencies of 8 Hz and 16 Hz, indicating a frequency-dependent relationship. At a high pacing rate of 16 Hz, alternans often converted into arrhythmia. An increase in AP alternans and arrhythmic events occurred in all regions (LV, septum and RV) during incremental pacing from 8 Hz to 16 Hz frequency (Fig. 5B). Transmural heterogeneities were observed in the LV free wall, with greater AP alternans and arrhythmic events in the endocardium in comparison with epicardium at both 8 Hz and 16 Hz frequencies (Fig. 5B; $P < 0.05$, $n = 6$ hearts). There are no significant interventricular differences observed in the incidence of AP alternans, with a similar number occurring in the left ventricle, right ventricle and septum at both 8 Hz and 16 Hz frequencies.

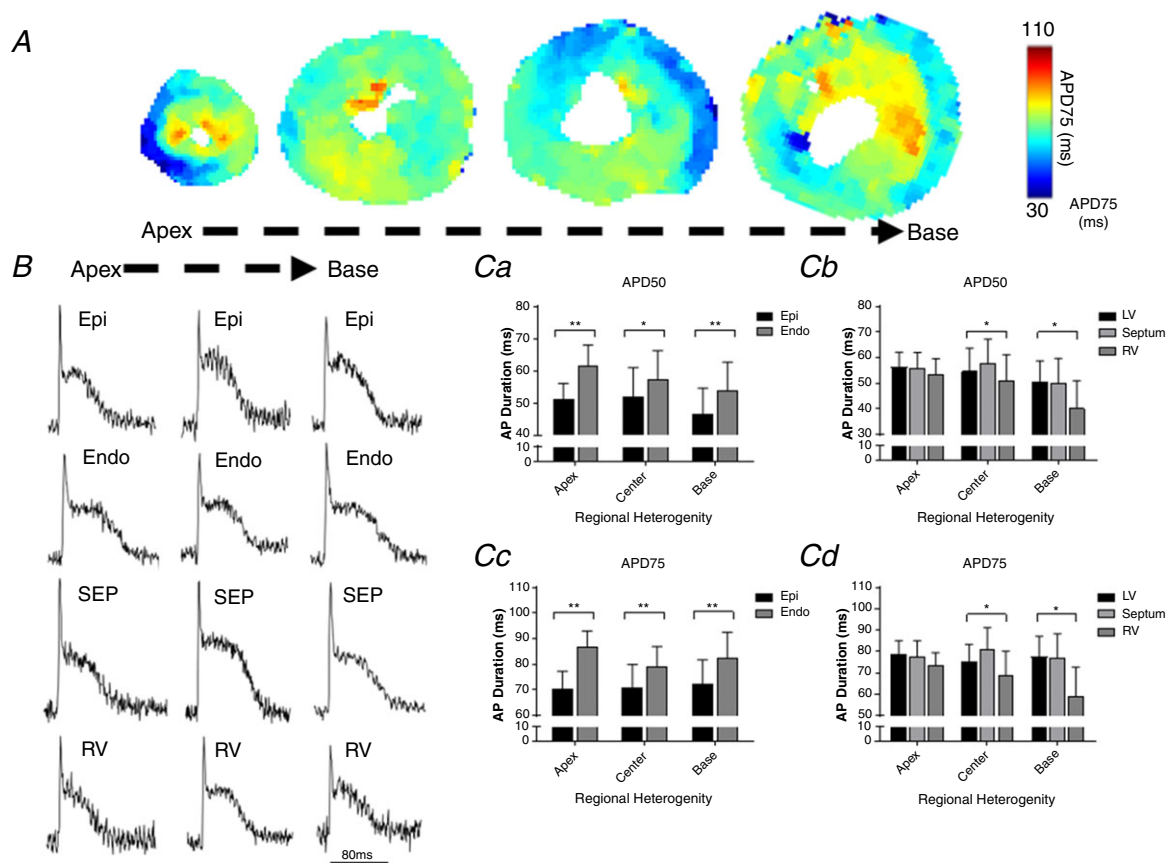


Figure 3. Transmural and regional distribution of AP duration across the murine ventricles
 A, representative maps of AP duration (APD75) at 2 Hz pacing frequency (500 ms pacing cycle length) recorded from apex to base in transverse ventricular slices. B, typical optical AP recordings (unfiltered signals) obtained from different regions of the murine ventricles at 2 Hz pacing frequency. Scale bar: 80 ms. C, quantitative summary of transmural and regional APD50 (Ca and Cb) and APD75 distribution (Cc and Cd) at 2 Hz pacing ($n = 5$ hearts; $**P < 0.01$; $*P < 0.05$). Values expressed as means \pm SEM. Epi, epicardium; Endo, endocardium; SEP, septum; RV, right ventricle; LV, left ventricle.

Figure 6 illustrates the activation maps generated within bespoke ElectroMap analysis software (O'Shea *et al.* 2017). A polynomial surface was then fitted to local activation times to describe propagation in the area, and local CV quantified as the gradient vector of the polynomial surface. Mean CV was then calculated from the local CVs across the tissue slice. As seen in Fig. 6, there is a clear slowing of conduction at higher pacing frequencies. This is apparent when CV data is analysed across all the slices (Fig. 6A-C) or across individual hearts (Fig. 6A-C). In some slices we analysed there is evidence of steep activation gradients and focal activity, which may contribute to the arrhythmias observed.

As shown in Fig. 7B, a significant increase in CaT alternans and arrhythmic events occurred in the epicardium and endocardium of the left ventricle, in the ventricular septum and in the right ventricle with increase of pacing frequency from 8 Hz to 16 Hz. Transmural heterogeneities were also observed, with lower occurrence of CaT alternans and arrhythmic events in the epicardium

in comparison with endocardium at both 8 Hz and 16 Hz frequencies (Fig. 7B; $P < 0.05$, $n = 6$ hearts).

Discussion

In the present study we developed and validated a transverse ventricular tissue slice model to enable systematic analysis of V_m and CaT across the whole murine ventricles. Our investigation of murine transverse slices, prepared from both ventricles (from apex to base) combined with high resolution optical mapping, revealed transmural and regional heterogeneities in both physiological APD and CaTD, and in the incidence of frequency-dependent AP and CaT alternans in the murine ventricles.

Optimisation of cardiac slices for V_m and CaT measurements

Cardiac slice technology has previously been employed for structural and functional studies of human biopsies

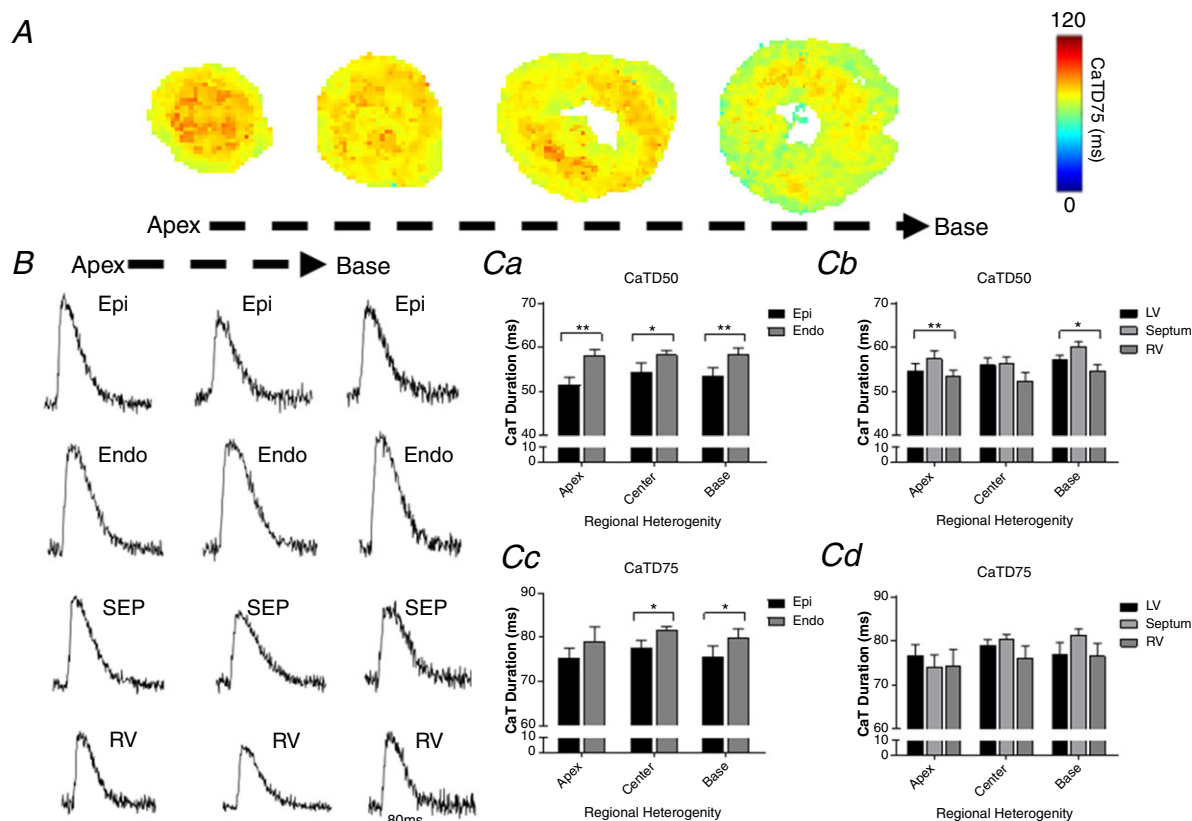


Figure 4. Transmural and regional distribution of CaT duration in the murine ventricles

A, representative maps of CaT duration (CaTD75) at 2 Hz pacing frequency (500 ms pacing cycle length) recorded from apex to base in transverse ventricular slices. **B**, representative optical CaT raw traces obtained from different regions of the murine ventricles at 2 Hz pacing frequency. Scale bar: 80 ms. **C**, quantitative summary of transmural and regional CaTD50 (**Ca** and **Cb**) and CaTD75 distribution (**Cc** and **Cd**) at 2 Hz pacing ($n = 5-8$ hearts; $**P < 0.01$; $*P < 0.05$). Values expressed as means \pm SEM. Epi, epicardium; Endo, endocardium; SEP, septum; RV, right ventricle; LV, left ventricle.

and animal hearts (Halbach *et al.* 2006; Bussek *et al.* 2009; Camelliti *et al.* 2011), but application of the preparation in optical mapping studies is only starting to emerge (Wang *et al.* 2015; Kang *et al.* 2016). This report is the first to present a detailed protocol for successful preparation of transverse ventricular slices for transmural and regional profiling of V_m and CaT with high resolution optical mapping. Important steps include dye loading via Langendorff perfusion; slice cutting perpendicular to the long axis of the heart; a slice thickness of 300 μm ; and a post-cutting recovery period of 30 min.

In contrast to prior reports of cardiac slice preparation, slices were cut at right angles to the long axis of the heart (transverse slices) and not tangentially to the epicardial

surface (Bussek *et al.* 2009; Camelliti *et al.* 2011). This allowed us to prepare a complete series of slices containing left ventricle, right ventricle and ventricular septum regions from apex to base. Given the curvature of the mouse ventricles and the different thickness of LV, RV and septum at the apex and base, preparing tangential slices containing well aligned cardiomyocytes covering the entire ventricular tissue, for the study of transmural and regional heterogeneities, was not feasible. Importantly our study demonstrates that transverse mouse slices are viable and show robust voltage and calcium signals. We identified slice thickness as a critical parameter for successful preparation of viable transverse slices. Previous studies have reported thicknesses from 150 to 500 μm (Pertsov *et al.*

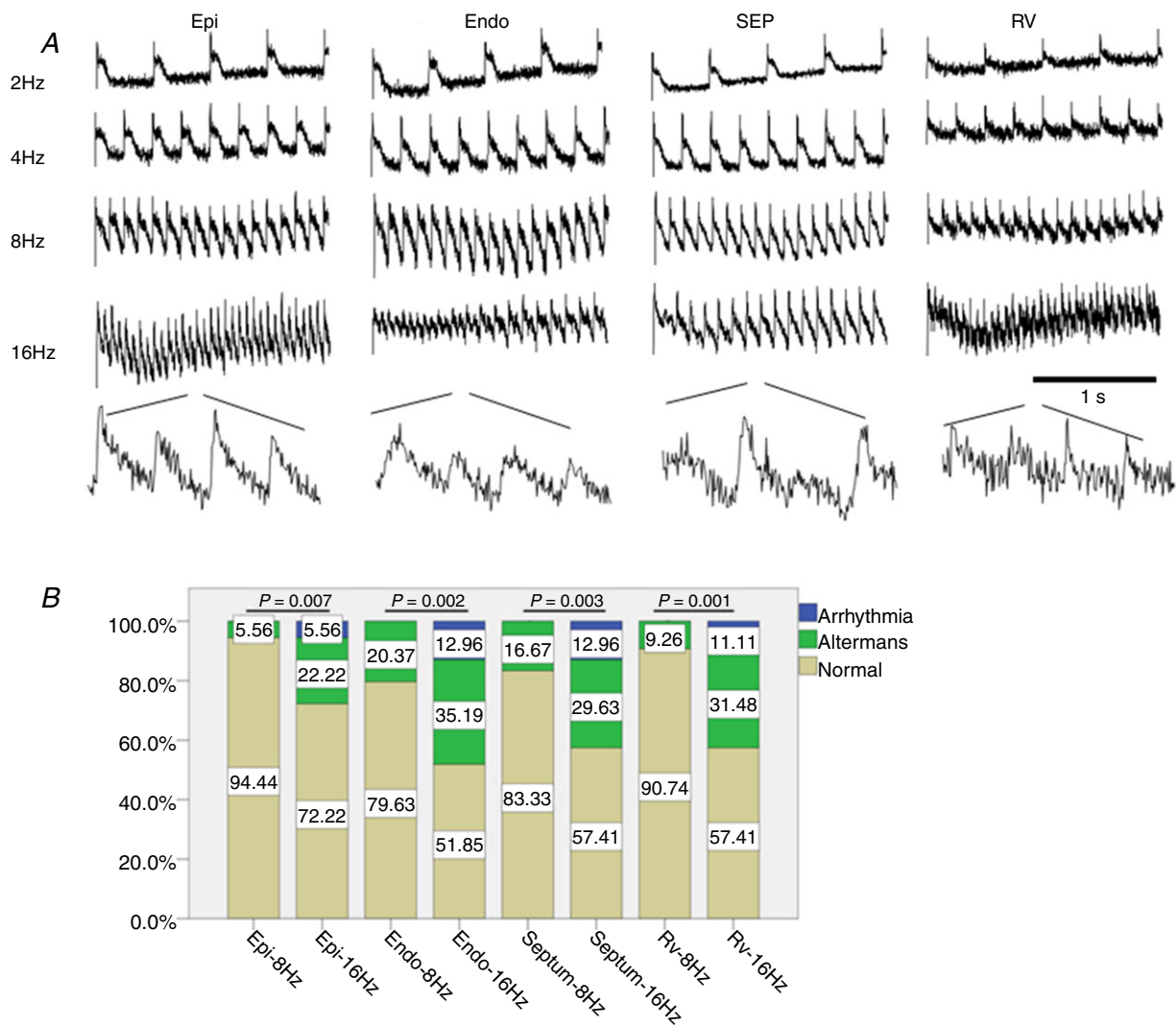


Figure 5. Regional and frequency-dependent distribution of AP alternans and arrhythmic events in murine ventricular slices

A, representative optical AP traces obtained from different regions within a ventricular slice during electrical pacing at 2, 4, 8 and 16 Hz frequency. Scale bar: 1 s. B, transmural and regional occurrence of alternans and arrhythmias at 8 Hz and 16 Hz pacing frequency. Epi, epicardium; Endo, endocardium; SEP, septum; RV, right ventricle; LV, left ventricle. $n = 6$ hearts.

1993; Halbach *et al.* 2006; Camelliti *et al.* 2011; Wang *et al.* 2015), but in this study we determined that 300 μm was the best slice thickness to guarantee cell viability and achieve optimal V_m and Ca^{2+} signals using optical mapping techniques. Transverse slices less than 300 μm showed significantly reduced V_m and CaT signals (Fig. 1E). We suggest that, with mouse ventricular myocyte dimensions estimated as 90 μm (length) \times 25 μm (width) (Toischer *et al.* 2010), overly thin slices may result in damage to the vast majority of available cells within the slice. Slices thicker than 400 μm , on the other hand, required larger electrical stimulation pulses, longer post-cutting recovery time, and suffered from poor oxygenation and limited BDM washout. BDM, if not completely washed out, is known to have residual effects on cardiac ion channels (Coulombe *et al.* 1990). Oxygen supply, in the absence of vascular perfusion, is guaranteed by diffusion in cardiac slices. However, as the maximum diffusion distance for cardiac contracting muscle is estimated to be 150 μm (Barclay, 2005), slices thicker than 300 μm will be exposed to hypoxic conditions, resulting in limited viability.

In previous studies, post-cutting recovery times ranging from 30 min (Burnashev *et al.* 1990) to 2 h (Yasuhara *et al.* 1996) were reported. For transverse mouse ventricular slices we determined an optimal recovery period to be 30 min. Slices cut in cold (4°C), oxygenated (99.5%

O_2) Tyrode solution containing BDM were placed in Krebs solution containing 10 μM blebbistatin at room temperature (equilibrated with 95% O_2 /5% CO_2) to recover. The recovery time of 30 min allowed washout of BDM and returned the slices to a more physiological temperature. Our findings are consistent with previous reports indicating recovery times for adult guinea-pig slices and neonatal rat slices of, respectively, 36 min (Wang *et al.* 2015) and 30 min (Pertsov *et al.* 1993; Davidenko *et al.* 1995).

Conduction velocity as an indicator of physiological state is shown in Fig. 6. We demonstrate that conduction velocity in our cardiac slices is comparable to conduction velocity measured in whole mouse hearts by epicardial optical mapping (Baker *et al.* 2000; Baudenbacher *et al.* 2008; Myles *et al.* 2012; Bao *et al.* 2016). As expected, higher pacing frequencies lead to reduced conduction velocities, further demonstrating physiological responsiveness of the slices (Weber *et al.* 2011).

Cardiac slices for the study of transmural and regional heterogeneity of V_m and CaT

A critical advantage of the cardiac slice model is the ability to provide access to any region of the ventricles, thus enabling exploration of regional and transmural

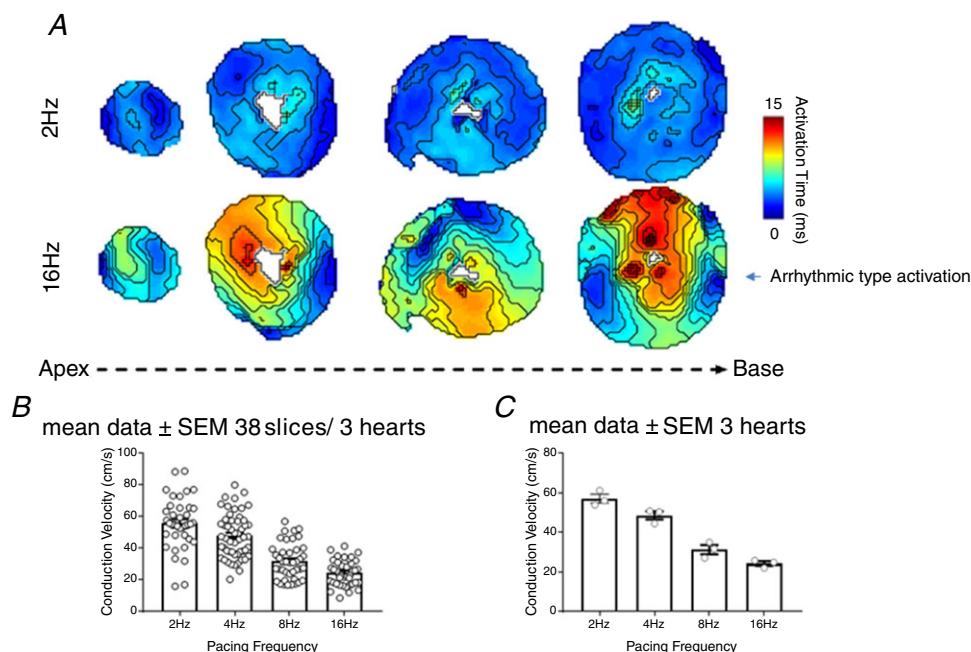


Figure 6. Analysis of conduction velocity (CV)

A, activation maps of slices (apex to base) paced at 2 Hz and 16 Hz. Conduction velocity (CV) was calculated using a multi-vector polynomial method within bespoke ElectroMap analysis software. A polynomial surface was fitted to local activation times to describe propagation in the area, and local CV quantified as the gradient vector of the polynomial surface. Mean CV was then calculated from the local CVs across the tissue slice. B, mean data for CV at a range of pacing frequencies calculated across all the slices ($n = 38$ slices/3 hearts). C, mean data for CV at a range of pacing frequencies calculated across all the hearts ($n = 3$ hearts).

differences. This is particularly important for the mouse heart, given that other *in vitro* tissue preparations, such as ventricular wedges, are not feasible for small hearts.

Action potential and calcium handling heterogeneities, and their role in the generation of arrhythmias, are well documented in hearts from larger mammals (Yan *et al.* 1998; Burton & Cobbe, 2001; Laurita *et al.* 2003; Cordeiro *et al.* 2004; Patel *et al.* 2009; Glukhov *et al.* 2010; Lou *et al.* 2011). However, experimental data on transmural and regional electrophysiological characteristics in the murine heart are still limited. In this study we have combined transverse murine cardiac slices with high resolution optical mapping for systematic transmural and regional profiling of both V_m and CaT across the murine ventricles. Our results indicate the presence of transmural

APD heterogeneities within the wall of the left ventricle (Fig. 3), with the shortest APD observed in the epicardium, in agreement with previously published results for single isolated myocytes (Brunet *et al.* 2004) and ventricular tissue (Knollmann *et al.* 2001). However, no significant apico-basal APD gradients were found in our study (Fig. 3), in contrast with previously reported findings on single isolated myocytes (Xu *et al.* 1999; Bondarenko *et al.* 2004). Transmural and apico-basal gradients in the transient outward K^+ current (I_{to}) are thought to be the main determinant of APD heterogeneities in the mouse ventricle (Xu *et al.* 1999; Brunet *et al.* 2004; Rossow *et al.* 2006).

Our results also indicate the presence of significant interventricular differences in APD, with shorter APD in the right ventricle in comparison to the left ventricle and

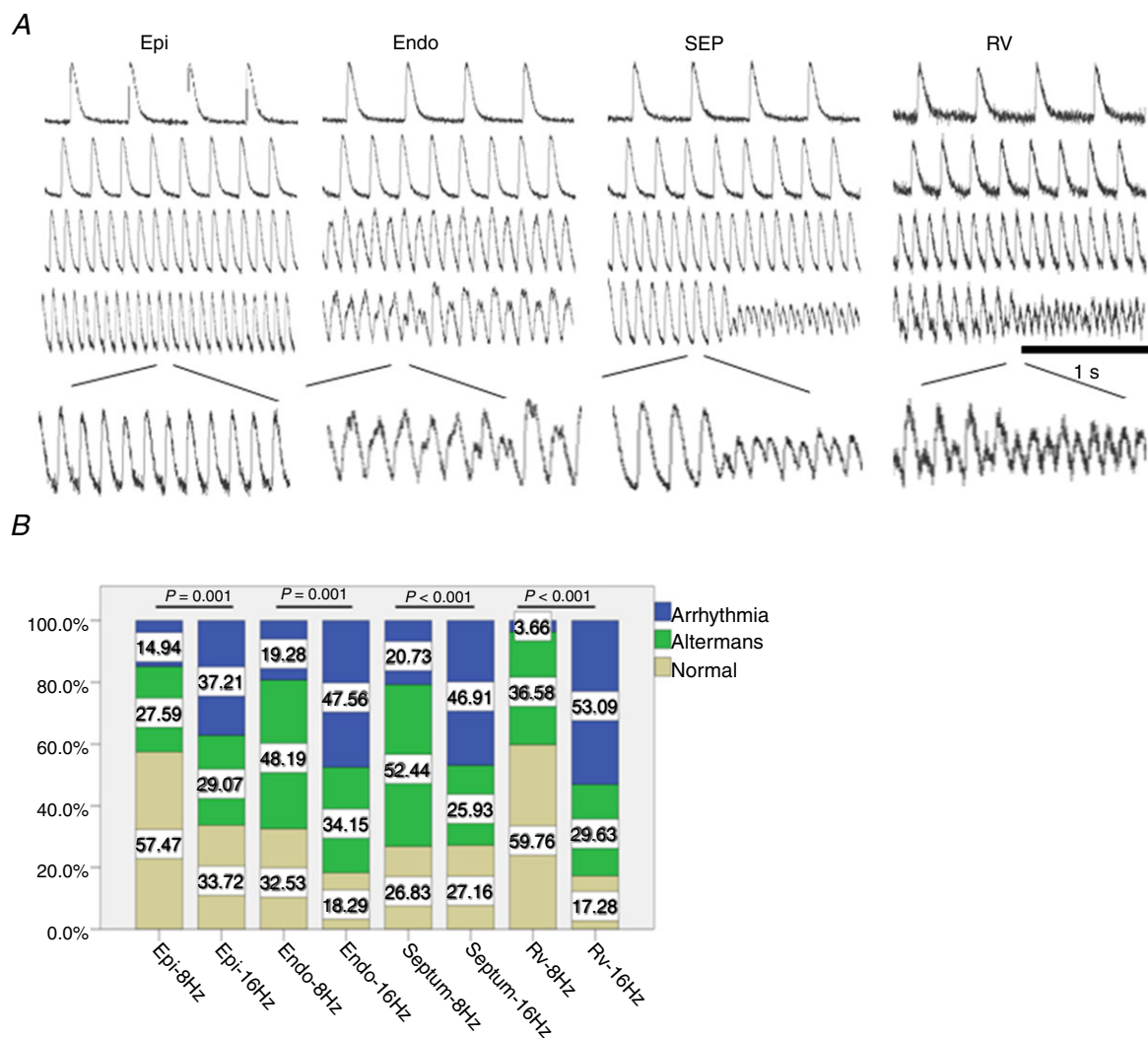


Figure 7. Regional and frequency-dependent distribution of CaT alternans and arrhythmic events in murine ventricular slices

A, representative optical CaT traces obtained from different regions within a ventricular slice during electrical pacing at 2, 4, 8 and 16 Hz frequency. Scale bar: 1s. B, transmural and regional occurrence of alternans and arrhythmias at 8 Hz and 16 Hz pacing frequency. Epi, epicardium; Endo, endocardium; SEP, septum; RV, right ventricle; LV, left ventricle. *n* = 6 hearts.

ventricular septum (Fig. 3). This is in agreement with data from rodent studies (Watanabe *et al.* 1983; Knollmann *et al.* 2001) and larger mammals investigations (Di Diego *et al.* 1996; Volders *et al.* 1999), and it is likely to be the result of differences in repolarisation currents which are significantly higher in cells isolated from the right than the left ventricle (Brunet *et al.* 2004; Molina *et al.* 2016).

Analysis of Ca^{2+} transients revealed the presence of transmural and regional heterogeneity of calcium handling in the murine ventricles, in addition to action potential gradients. A significant transmural gradient of CaTD50 and CaTD75 was found in the LV wall, with a longer CaTD in the endocardium compared to the epicardium (Fig. 4). Similar results have been reported for hearts of other species (Figueredo *et al.* 1993; Laurita *et al.* 2003). Regional differences in the expression of calcium regulatory proteins could explain the observed transmural CaTD heterogeneity. Differences in sarcoplasmic reticulum Ca^{2+} -ATPase (SERCA2a) and ryanodine receptor type 2 (RyR2) protein expression, and sodium–calcium exchanger function, have been reported between epicardial and endocardial cells in different species including mouse (Laurita *et al.* 2003; Cordeiro *et al.* 2004; Dilly *et al.* 2006; Lou *et al.* 2011). We also observed interventricular differences in CaTD50 in our study, with a shorter CaTD50 in the right ventricle in comparison to the left ventricle and ventricular septum (Fig. 4), consistent with previously reported interventricular differences in Ca^{2+} handling and contractility in rodent hearts (Kondo *et al.* 2006; Molina *et al.* 2016).

AP and CaT alternans during rapid pacing

Cardiac alternans in the form of T-wave alternans in the ECG, corresponding to beat-to-beat alternations in ventricular repolarisation, has demonstrated clinical utility in stratifying risk for malignant arrhythmias and sudden cardiac death, providing guidance for anti-arrhythmic therapy (Verrier *et al.* 2011). At the cellular level, cardiac alternans manifests as rate-dependent beat-to-beat alternations in contraction, AP morphology and CaT amplitude (Kanaporis & Blatter, 2015). In our study, we observed alternans in AP amplitude as well as in CaT amplitude when murine slices were electrically stimulated at high pacing rates (Figs 5 and 6). Alternans in AP amplitude have been reported previously in left ventricular wedge preparations from normal and post-infarction rabbit hearts during rapid pacing (Myles *et al.* 2011). Importantly, alternans in AP amplitude were related to the development of arrhythmias during rapid pacing in the rabbit wedge, indicating that amplitude alternans may be an important mechanism for ventricular arrhythmia (Myles *et al.* 2011). As we demonstrated in Figs 5–7, arrhythmia was clearly triggered by high

pacing frequency, when we observed reduced conduction velocities and areas of steep activation gradients. The majority of the events we observed were the non-sustained ventricular tachycardia (VT) form; such non-sustained VT is likely to be caused by focal activity and steep activation gradients.

Our results indicate the presence of significant transmural differences in pacing-induced AP and CaT alternans in the mouse LV free wall, with greater incidence of alternans in the endocardium compared with the epicardium at both 8 Hz and 16 Hz pacing frequencies (Figs 5B and 7B). To the best of our knowledge, this is the first report describing transmural heterogeneities in frequency-dependent AP and CaT alternans in the murine heart. Regional differences in CaT alternans have been previously described in the canine LV during rapid pacing in studies using wedge preparations and isolated myocytes (Laurita *et al.* 2003; Cordeiro *et al.* 2007). In these published studies, larger levels of alternans were observed in cells near the endocardium compared with cells near the epicardium (Laurita *et al.* 2003; Cordeiro *et al.* 2007), consistent with the findings of our study.

In the current study, we observed similar transmural and regional distributions of AP and CaT alternans. Electrical and CaT alternans are known to be highly correlated, although it remains controversial whether the primary cause of cardiac alternans is a disturbance of intracellular Ca^{2+} signalling or electrical membrane properties. In a recent study by Kanaporis and Blatter (2015), the mechanisms of calcium cycling and action potential dynamics in cardiac alternans have been investigated in single rabbit atrial and ventricular myocytes using combined $[\text{Ca}^{2+}]_i$ and electrophysiological measurements. The findings indicate that suppression of Ca^{2+} release from the sarcoplasmic reticulum abolished APD alternans, supporting a central role for intracellular Ca^{2+} cycling in the development of cardiac alternans (Kanaporis & Blatter, 2015). Cardiac slices, simultaneously loaded with voltage- and Ca^{2+} -sensitive dyes, will allow us to examine the cellular mechanisms of cardiac alternans in a more representative multicellular model system.

Study limitations

A limitation to the study is the possibility of injury and uncoupling; partial uncoupling (reduction in conductance) could increase the differences in APDs between epicardial and endocardial regions.

Conclusions

We have developed and validated a robust experimental methodology which combines transverse ultra-thin cardiac slices and high resolution optical mapping to

enable systematic analysis of transmural and regional gradients in V_m and CaT across the entire murine ventricles.

References

- Asano Y, Takashima S, Asakura M, Shintani Y, Liao Y, Minamino T, Asanuma H, Sanada S, Kim J, Ogai A, Fukushima T, Oikawa Y, Okazaki Y, Kaneda Y, Sato M, Miyazaki J, Kitamura S, Tomoike H, Kitakaze M & Hori M (2004). Lamr1 functional retroposon causes right ventricular dysplasia in mice. *Nat Genet* **36**, 123–130.
- Baker LC, London B, Choi BR, Koren G & Salama G (2000). Enhanced dispersion of repolarization and refractoriness in transgenic mouse hearts promotes reentrant ventricular tachycardia. *Circ Res* **86**, 396–407.
- Bao Y, Willis BC, Frasier CR, Lopez-Santiago LF, Lin X, Ramos-Mondragon R, Auerbach DS, Chen C, Wang Z, Anumonwo J, Valdivia HH, Delmar M, Jalife J & Isom LL (2016). Scn2b deletion in mice results in ventricular and atrial arrhythmias. *Circu Arrhythm Electrophysiol* **9**, e003923.
- Barclay CJ (2005). Modelling diffusive O₂ supply to isolated preparations of mammalian skeletal and cardiac muscle. *J Muscle Res Cell Motil* **26**, 225–235.
- Baudenbacher F, Schober T, Pinto JR, Sidorov VY, Hilliard F, Solaro RJ, Potter JD & Knollmann BC (2008). Myofibrillar Ca²⁺ sensitization causes susceptibility to cardiac arrhythmia in mice. *J Clin Invest* **118**, 3893–3903.
- Bayly PV, KenKnight BH, Rogers JM, Hillsley RE, Ideker RE & Smith WM (1998). Estimation of conduction velocity vector fields from epicardial mapping data. *IEEE Trans Biomed Eng* **45**, 563–571.
- Bondarenko VE, Szigeti GP, Bett GC, Kim SJ & Rasmusson RL (2004). Computer model of action potential of mouse ventricular myocytes. *Am J Physiol Heart Circ Physiol* **287**, H1378–H1403.
- Brunet S, Aimond F, Li H, Guo W, Eldstrom J, Fedida D, Yamada KA & Nerbonne JM (2004). Heterogeneous expression of repolarizing, voltage-gated K⁺ currents in adult mouse ventricles. *J Physiol* **559**, 103–120.
- Burnashev NA, Edwards FA & Verkhratsky AN (1990). Patch-clamp recordings on rat cardiac muscle slices. *Pflugers Arch* **417**, 123–125.
- Burton FL & Cobbe SM (2001). Dispersion of ventricular repolarization and refractory period. *Cardiovasc Res* **50**, 10–23.
- Bussek A, Wettwer E, Christ T, Lohmann H, Camelliti P & Ravens U (2009). Tissue slices from adult mammalian hearts as a model for pharmacological drug testing. *Cell Physiol Biochem* **24**, 527–536.
- Camelliti P, Al-Saud SA, Smolenski RT, Al-Ayoubi S, Bussek A, Wettwer E, Banner NR, Bowles CT, Yacoub MH & Terracciano CM (2011). Adult human heart slices are a multicellular system suitable for electrophysiological and pharmacological studies. *J Mol Cell Cardiol* **51**, 390–398.
- Choy L, Yeo JM, Tse V, Chan SP & Tse G (2016). Cardiac disease and arrhythmogenesis: Mechanistic insights from mouse models. *Int J Cardiol Heart Vasc* **12**, 1–10.
- Cordeiro JM, Greene L, Heilmann C, Antzelevitch D & Antzelevitch C (2004). Transmural heterogeneity of calcium activity and mechanical function in the canine left ventricle. *Am J Physiol Heart Circ Physiol* **286**, H1471–H1479.
- Cordeiro JM, Malone JE, Di Diego JM, Scornik FS, Aistrup GL, Antzelevitch C & Wasserstrom JA (2007). Cellular and subcellular alternans in the canine left ventricle. *Am J Physiol Heart Circ Physiol* **293**, H3506–H3516.
- Coulombe A, Lefevre IA, Deroubaix E, Thuringer D & Coraboeuf E (1990). Effect of 2,3-butanedione 2-monoxime on slow inward and transient outward currents in rat ventricular myocytes. *J Mol Cell Cardiol* **22**, 921–932.
- Davidenko JM, Salomonsz R, Pertsov AM, Baxter WT & Jalife J (1995). Effects of pacing on stationary reentrant activity. Theoretical and experimental study. *Circ Res* **77**, 1166–1179.
- Di Diego JM, Sun ZQ & Antzelevitch C (1996). I_{to} and action potential notch are smaller in left vs. right canine ventricular epicardium. *Am J Physiol* **271**, H548–H561.
- Dilly KW, Rossow CF, Votaw VS, Meabon JS, Cabarrus JL & Santana LF (2006). Mechanisms underlying variations in excitation-contraction coupling across the mouse left ventricular free wall. *J Physiol* **572**, 227–241.
- Figueredo VM, Brandes R, Weiner MW, Massie BM & Camacho SA (1993). Endocardial versus epicardial differences of intracellular free calcium under normal and ischemic conditions in perfused rat hearts. *Circ Res* **72**, 1082–1090.
- Grundy D (2015). Principles and standards for reporting animal experiments in *The Journal of Physiology* and *Experimental Physiology*. *J Physiol* **593**, 2547–2549.
- Glukhov AV, Fedorov VV, Lou Q, Ravikumar VK, Kalish PW, Schuessler RB, Moazami N & Efimov IR (2010). Transmural dispersion of repolarization in failing and nonfailing human ventricle. *Circ Res* **106**, 981–991.
- Halbach M, Pillekamp F, Brockmeier K, Hescheler J, Muller-Ehmsen J & Reppel M (2006). Ventricular slices of adult mouse hearts—a new multicellular in vitro model for electrophysiological studies. *Cell Physiol Biochem* **18**, 1–8.
- Himmel HM, Bussek A, Hoffmann M, Beckmann R, Lohmann H, Schmidt M & Wettwer E (2012). Field and action potential recordings in heart slices: correlation with established in vitro and in vivo models. *Br J Pharmacol* **166**, 276–296.
- Kanaporis G & Blatter LA (2015). The mechanisms of calcium cycling and action potential dynamics in cardiac alternans. *Circ Res* **116**, 846–856.
- Kang C, Qiao Y, Li G, Baechle K, Camelliti P, Rentschler S & Efimov IR (2016). Human organotypic cultured cardiac slices: new platform for high throughput preclinical human trials. *Sci Rep* **6**, 28798.
- Knollmann BC, Katchman AN & Franz MR (2001). Monophasic action potential recordings from intact mouse heart: validation, regional heterogeneity, and relation to refractoriness. *J Cardiovasc Electrophysiol* **12**, 1286–1294.
- Kondo RP, Dederko DA, Teutsch C, Chrast J, Catalucci D, Chien KR & Giles WR (2006). Comparison of contraction and calcium handling between right and left ventricular myocytes from adult mouse heart: a role for repolarization waveform. *J Physiol* **571**, 131–146.

- Lander ES, Linton LM, Birren B, Nusbaum C, Zody MC, Baldwin J, Devon K, Dewar K, Doyle M, FitzHugh W, Funke R, Gage D, Harris K, Heaford A, Howland J, Kann L, Lehoczky J, LeVine R, McEwan P, McKernan K, Meldrim J, Mesirov JP, Miranda C, Morris W, Naylor J, Raymond C, Rosetti M, Santos R, Sheridan A, Sougnez C, Stange-Thomann Y, Stojanovic N, Subramanian A, Wyman D, Rogers J, Sulston J, Ainscough R, Beck S, Bentley D, Burton J, Clee C, Carter N, Coulson A, Deadman R, Deloukas P, Dunham A, Dunham I, Durbin R, French L, Grafham D, Gregory S, Hubbard T, Humphray S, Hunt A, Jones M, Lloyd C, McMurray A, Matthews L, Mercer S, Milne S, Mullikin JC, Mungall A, Plumb R, Ross M, Shownkeen R, Sims S, Waterston RH, Wilson RK, Hillier LW, McPherson JD, Marra MA, Mardis ER, Fulton LA, Chinwalla AT, Pepin KH, Gish WR, Chissole SL, Wendl MC, Delehaunty KD, Miner TL, Delehaunty A, Kramer JB, Cook LL, Fulton RS, Johnson DL, Minx PJ, Clifton SW, Hawkins T, Branscomb E, Predki P, Richardson P, Wenning S, Slezak T, Doggett N, Cheng JF, Olsen A, Lucas S, Elkin C, Uberbacher E, Frazier M, Gibbs RA, Muzny DM, Scherer SE, Bouck JB, Sodergren EJ, Worley KC, Rives CM, Gorrell JH, Metzker ML, Naylor SL, Kucherlapati RS, Nelson DL, Weinstock GM, Sakaki Y, Fujiyama A, Hattori M, Yada T, Toyoda A, Itoh T, Kawagoe C, Watanabe H, Totoki Y, Taylor T, Weissenbach J, Heilig R, Saurin W, Artiguenave F, Brottier P, Bruls T, Pelletier E, Robert C, Wincker P, Smith DR, Doucette-Stamm L, Rubenfield M, Weinstock K, Lee HM, Dubois J, Rosenthal A, Platzer M, Nyakatura G, Taudien S, Rump A, Yang H, Yu J, Wang J, Huang G, Gu J, Hood L, Rowen L, Madan A, Qin S, Davis RW, Federspiel NA, Abola AP, Proctor MJ, Myers RM, Schmutz J, Dickson M, Grimwood J, Cox DR, Olson MV, Kaul R, Raymond C, Shimizu N, Kawasaki K, Minoshima S, Evans GA, Athanasiou M, Schultz R, Roe BA, Chen F, Pan H, Ramser J, Lehrach H, Reinhardt R, McCombie WR, de la Bastide M, Dedhia N, Blocker H, Hornischer K, Nordsiek G, Agarwala R, Aravind L, Bailey JA, Bateman A, Batzoglou S, Birney E, Bork P, Brown DG, Burge CB, Cerutti L, Chen HC, Church D, Clamp M, Copley RR, Doerks T, Eddy SR, Eichler EE, Furey TS, Galagan J, Gilbert JG, Harmon C, Hayashizaki Y, Haussler D, Hermjakob H, Hokamp K, Jang W, Johnson LS, Jones TA, Kasif S, Kasprzyk A, Kennedy S, Kent WJ, Kitts P, Koonin EV, Korf I, Kulp D, Lancet D, Lowe TM, McLysaght A, Mikkelsen T, Moran JV, Mulder N, Pollara VJ, Ponting CP, Schuler G, Schultz J, Slater G, Smit AF, Stupka E, Szustakowski J, Thierry-Mieg D, Thierry-Mieg J, Wagner L, Wallis J, Wheeler R, Williams A, Wolf YI, Wolfe KH, Yang SP, Yeh RF, Collins F, Guyer MS, Peterson J, Felsenfeld A, Wetterstrand KA, Patrinos A, Morgan MJ, de Jong P, Catanese JJ, Osoegawa K, Shizuya H, Choi S, Chen YJ & Szustakowski J (2001). Initial sequencing and analysis of the human genome. *Nature* **409**, 860–921.
- Laurita KR, Katra R, Wible B, Wan X & Koo MH (2003). Transmural heterogeneity of calcium handling in canine. *Circ Res* **92**, 668–675.
- Lou Q, Fedorov VV, Glukhov AV, Moazami N, Fast VG & Efimov IR (2011). Transmural heterogeneity and remodeling of ventricular excitation-contraction coupling in human heart failure. *Circulation* **123**, 1881–1890.
- Molina CE, Heijman J & Dobrev D (2016). Differences in left versus right ventricular electrophysiological properties in cardiac dysfunction and arrhythmogenesis. *Arrhythm Electrophysiol Rev* **5**, 14–19.
- Myles RC, Burton FL, Cobbe SM & Smith GL (2011). Alternans of action potential duration and amplitude in rabbits with left ventricular dysfunction following myocardial infarction. *J Mol Cell Cardiol* **50**, 510–521.
- Myles RC, Wang L, Kang C, Bers DM & Ripplinger CM (2012). Local beta-adrenergic stimulation overcomes source-sink mismatch to generate focal arrhythmia. *Circ Res* **110**, 1454–1464.
- Nerbonne JM (2014). Mouse models of arrhythmogenic cardiovascular disease: challenges and opportunities. *Current Opin Pharmacol* **15**, 107–114.
- O'Shea C, Holmes A, Yu TY, Winter J, Correia J, Kirchhof P, Fabritz L, Rajpoot K & Pavlovic D (2017). 188 Development of a novel software package for high-throughput processing and analysis of cardiac optical mapping data. *Heart* **103**, A128–A129.
- Papadatos GA, Wallerstein PMR, Head CEG, Ratcliff R, Brady PA, Benndorf K, Saumarez RC, Trezise AEO, Huang CLH, Vandenberg JI, Colledge WH & Grace AA (2002). Slowed conduction and ventricular tachycardia after targeted disruption of the cardiac sodium channel gene Scn5a. *Proc Natl Acad Sci U S A* **99**, 6210–6215.
- Patel C, Burke JF, Patel H, Gupta P, Kowey PR, Antzelevitch C & Yan GX (2009). Is there a significant transmural gradient in repolarization time in the intact heart? Cellular basis of the T wave: a century of controversy. *Circ Arrhythm Electrophysiol* **2**, 80–88.
- Pertsov AM, Davidenko JM, Salomonsz R, Baxter WT & Jalife J (1993). Spiral waves of excitation underlie reentrant activity in isolated cardiac muscle. *Circ Res* **72**, 631–650.
- Rossow CF, Dilly KW & Santana LF (2006). Differential calcineurin/NFATc3 activity contributes to the Ito transmural gradient in the mouse heart. *Circ Res* **98**, 1306–1313.
- Sabir IN, Killeen MJ, Grace AA & Huang CL (2008). Ventricular arrhythmogenesis: insights from murine models. *Prog Biophys Mol Biol* **98**, 208–218.
- Toischer K, Rokita AG, Unsold B, Zhu W, Kararigas G, Sossalla S, Reuter SP, Becker A, Teucher N, Seidler T, Grebe C, Preuss L, Gupta SN, Schmidt K, Lehnart SE, Kruger M, Linke WA, Backs J, Regitz-Zagrosek V, Schafer K, Field LJ, Maier LS & Hasenfuss G (2010). Differential cardiac remodeling in preload versus afterload. *Circulation* **122**, 993–1003.
- Verrier RL, Klingenhoben T, Malik M, El-Sherif N, Exner DV, Hohnloser SH, Ikeda T, Martinez JP, Narayan SM, Nieminen T & Rosenbaum DS (2011). Microvolt T-wave alternans physiological basis, methods of measurement, and clinical utility – consensus guideline by International Society for Holter and Noninvasive Electrocardiology. *J Am Coll Cardiol* **58**, 1309–1324.
- Volders PG, Sipido KR, Carmeliet E, Spatjens RL, Wellens HJ & Vos MA (1999). Repolarizing K⁺ currents I_{TO1} and I_{Ks} are larger in right than left canine ventricular midmyocardium. *Circulation* **99**, 206–210.

- Wang K, Lee P, Mirams GR, Sarathchandra P, Borg TK, Gavaghan DJ, Kohl P & Bollensdorff C (2015). Cardiac tissue slices: preparation, handling, and successful optical mapping. *Am J Physiol Heart Circ Physiol* **308**, H1112–H1125.
- Wang K, Terrar D, Gavaghan DJ, Mu UMR, Kohl P & Bollensdorff C (2014). Living cardiac tissue slices: an organotypic pseudo two-dimensional model for cardiac biophysics research. *Prog Biophys Mol Biol* **115**, 314–327.
- Watanabe T, Delbridge LM, Bustamante JO & McDonald TF (1983). Heterogeneity of the action potential in isolated rat ventricular myocytes and tissue. *Circ Res* **52**, 280–290.
- Waterston RH, Lindblad-Toh K, Birney E, Rogers J, Abril JF, Agarwal P, Agarwala R, Ainscough R, Alexandersson M, An P, Antonarakis SE, Attwood J, Baertsch R, Bailey J, Barlow K, Beck S, Berry E, Birren B, Bloom T, Bork P, Botcherby M, Bray N, Brent MR, Brown DG, Brown SD, Bult C, Burton J, Butler J, Campbell RD, Carninci P, Cawley S, Chiaromonte F, Chinwalla AT, Church DM, Clamp M, Clee C, Collins FS, Cook LL, Copley RR, Coulson A, Couronne O, Cuff J, Curwen V, Cutts T, Daly M, David R, Davies J, Delehaunty KD, Deri J, Dermitzakis ET, Dewey C, Dickens NJ, Diekhans M, Dodge S, Dubchak I, Dunn DM, Eddy SR, Elnitski L, Emes RD, Eswara P, Eyas E, Felsenfeld A, Fewell GA, Flicek P, Foley K, Frankel WN, Fulton LA, Fulton RS, Furey TS, Gage D, Gibbs RA, Glusman G, Gnerre S, Goldman N, Goodstadt L, Grafham D, Graves TA, Green ED, Gregory S, Guigo R, Guyer M, Hardison RC, Haussler D, Hayashizaki Y, Hillier LW, Hinrichs A, Hlavina W, Holzer T, Hsu F, Hua A, Hubbard T, Hunt A, Jackson I, Jaffe DB, Johnson LS, Jones M, Jones TA, Joy A, Kamal M, Karlsson EK, Karolchik D, Kasprzyk A, Kawai J, Keibler E, Kells C, Kent WJ, Kirby A, Kolbe DL, Korfi I, Kucherlapati RS, Kulbokas EJ, Kulp D, Landers T, Leger JP, Leonard S, Letunic I, Levine R, Li J, Li M, Lloyd C, Lucas S, Ma B, Maglott DR, Mardis ER, Matthews L, Mauceli E, Mayer JH, McCarthy M, McCombie WR, McLaren S, McLay K, McPherson JD, Meldrim J, Meredith B, Mesirov JP, Miller W, Miner TL, Mongin E, Montgomery KT, Morgan M, Mott R, Mullikin JC, Muzny DM, Nash WE, Nelson JO, Nhan MN, Nicol R, Ning Z, Nusbaum C, O'Connor MJ, Okazaki Y, Oliver K, Overton-Larty E, Pachter L, Parra G, Pepin KH, Peterson J, Pevzner P, Plumb R, Pohl CS, Poliakov A, Ponce TC, Ponting CP, Potter S, Quail M, Reymond A, Roe BA, Roskin KM, Rubin EM, Rust AG, Santos R, Sapojnikov V, Schultz B, Schultz J, Schwartz MS, Schwartz S, Scott C, Seaman S, Searle S, Sharpe T, Sheridan A, Shownkeen R, Sims S, Singer JB, Slater G, Smit A, Smith DR, Spencer B, Stabenau A, Stange-Thomann N, Sugnet C, Suyama M, Tesler G, Thompson J, Torrents D, Trevaskis E, Tromp J, Ucla C, Ureta-Vidal A, Vinson JP, Von Niederhausern AC, Wade CM, Wall M, Weber RJ, Weiss RB, Wendl MC, West AP, Wetterstrand K, Wheeler R, Whelan S, Wierzbowski J, Willey D, Williams S, Wilson RK, Winter E, Worley KC, Wyman D, Yang S, Yang SP, Zdobnov EM, Zody MC & Lander ES (2002). Initial sequencing and comparative analysis of the mouse genome. *Nature* **420**, 520–562.
- Weber FM, Luik A, Schilling C, Seemann G, Krueger MW, Lorenz C, Schmitt C & Dossel O (2011). Conduction velocity restitution of the human atrium – an efficient measurement protocol for clinical electrophysiological studies. *IEEE Trans Biomed Eng* **58**, 2648–2655.
- Wehrens XH, Lehnart SE, Huang F, Vest JA, Reiken SR, Mohler PJ, Sun J, Guatimosim S, Song LS, Rosembli N, D'Armiento JM, Napolitano C, Memmi M, Priori SG, Lederer WJ & Marks AR (2003). FKBP12.6 deficiency and defective calcium release channel (ryanodine receptor) function linked to exercise-induced sudden cardiac death. *Cell* **113**, 829–840.
- Wu J, Zhang Y, Zhang X, Cheng L, Lammers WJEP, Grace AA, Fraser JA, Zhang H, Huang CLH & Lei M (2012). Altered sino-atrial node function and intra-atrial conduction in murine gain-of-function Scn5a+/delta KPQ hearts suggest an overlap syndrome. *Am J Physiol Heart Circ Physiol* **302**, H1510–H1523.
- Xu H, Guo W & Nerbonne JM (1999). Four kinetically distinct depolarization-activated K⁺ currents in adult mouse ventricular myocytes. *J Gen Physiol* **113**, 661–678.
- Yan GX, Shimizu W & Antzelevitch C (1998). Characteristics and distribution of M cells in arterially perfused canine left ventricular wedge preparations. *Circulation* **98**, 1921–1927.
- Yasuhara S, Takaki M, Kikuta A, Ito H & Suga H (1996). Myocardial VO₂ of mechanically unloaded contraction of rat ventricular slices measured by a new approach. *Am J Physiol Heart Circ Physiol* **270**, H1063–H1070.

Additional information

Competing interests

We confirm that none of the authors has any conflicts of interests on the submission form and in the manuscript.

Author contributions

Q.W, K.G, R.C, G.N and S.P: acquisition, analysis and/or interpretation of data for the work; G.H and C.OS: analysis and/or interpretation of data for the work, M.L and P.C: conception and design of the work, manuscript writing and revising it critically for important intellectual content; D.P, D.T, J,W and G.F: supporting the work and revising manuscript critically for important intellectual content. All authors have approved the final version of the manuscript and agree to be accountable for all aspects of the work. All persons designated as authors qualify for authorship, and all those who qualify for authorship are listed.

Funding

This study was supported by MRC (G1002647, G1002082; M.L.), BHF (PG/14/80/31106, PG/16/67/32340, PG/12/21/29473, PG/11/59/29004; M.L.), BHF CRE at Oxford (M.L.) grants.